Applied Soft Computing 46 (2016) 767–777

Contents lists available at ScienceDirect

Applied Soft Computing

journal homepage: www.elsevier.com/locate/asoc

A multiobjective fuzzy clustering method for change detection in SAR images☆

Hao Li, Maoguo Gong*, Qiao Wang, Jia Liu, Linzhi Su

Key Laboratory of Intelligent Perception and Image Understanding of Ministry of Education, Xidian University, No. 2 South TaiBai Road, Xi'an 710071, China

ARTICLE INFO

Article history:
Available online 27 November 2015

Keywords:
Image change detection
Synthetic Aperture Radar
Multi-objective optimization
Evolutionary algorithm

ABSTRACT

On account of the presence of speckle noise, the trade-off between removing noise and preserving detail is crucial for the change detection task in Synthetic Aperture Radar (SAR) images. In this paper, we put forward a multiobjective fuzzy clustering method for change detection in SAR images. The change detection problem is modeled as a multiobjective optimization problem, and two conflicting objective functions are constructed from the perspective of preserving detail and removing noise, respectively. We optimize the two constructed objective functions simultaneously by using a multiobjective fuzzy clustering method, which updates the membership values according to the weights of the two objectives to find the optimal trade-off. The proposed method obtains a set of solutions with different trade-off relationships between the two objectives, and users can choose one or more appropriate solutions according to requirements for diverse problems. Experiments conducted on real SAR images demonstrate the superiority of the proposed method.

1. Introduction

In recent years, Synthetic Aperture Radar (SAR) technology has been developed rapidly, the spaceborne SAR systems have observed the surface of the earth for years, and have acquired a plenty of multitemporal ground observation data. Many remote sensing studies have attempted to develop the techniques which can make good use of the information obtained by the SAR systems, including target extraction, object classification, edge detection, interferometry, change detection, etc. Among these studies, change detection technology has attracted widespread interests. Image change detection is based on the comparative analysis of multiple images acquired from the same area at different times with the purpose of detecting the change region between them [1]. In the past decades, the techniques for change detection in SAR images have found a wide range of applications, such as forest monitoring, urban studies, crop survey, and environmental monitoring [2–15].

As described in the literature [2], a change detection method generally consists of three main steps. The first step is image preprocessing, which mainly contains the image co-registration, noise reduction, radiometric correction and digital geometric correction. The second step is the acquisition of the difference image between the two images remaining to be detected. It is usually implemented by exploiting change detection operators with different features, such as the difference operator, the ratio operator and the log-ratio operator. The last step is the analysis of the difference image. In this step, changed regions are usually detected by employing a specific method. When we determine changed and unchanged areas by virtue of the comparative analysis of two SAR images, the change detection problems usually can be converted into binary classification problems. Two common approaches, the thresholding and the clustering approaches, are often used in this step. In a thresholding method, an appropriate decision threshold is applied to the gray level histogram of the generated difference image to divide the image into two classes. Many thresholding methods have been put forward, including Otsu, the Kittler and Illingworth minimum-error thresholding algorithm (K&I) and the expectation maximization (EM) algorithm [16]. The decision of an accurate model to be fit the two classes is difficult for the presence of speckle noise. The fuzzy c-means (FCM) algorithm is one of the most popular clustering methods, which can retain more information than hard clustering in some cases. However, the standard FCM algorithm is very sensitive to noise since it does not consider any information about spatial context. In recent years, many researchers have incorporated the local spatial and local grey level information into the original FCM algorithm to compensate this defect of FCM [17–21,12,14]. In [17], Ahmed et al. proposed FCM-S where the objective function of the standard FCM is modified to compensate for such inhomogeneities and to allow the labelling of a pixel to be influenced by the labels in its immediate neighborhood. One disadvantage of FCM-S is very time-consuming. Then Chen and Zhang [18] proposed two variants of FCM-S (FCM-S1 and FCM-S2) algorithm in order to reduce the computation time. These two algorithm respectively introduced the extra mean and median-filtered image, which can be computed in advance to replace the neighborhood term of FCM-S. Then a lot of other approaches have been proposed, such as the enhanced FCM algorithm (EnFCM) [21], the fast generalized FCM algorithm (FGFCM) [19]. In [20], Krindis and Chatzis proposed a robust fuzzy local information c-means clustering algorithm (FLICM), which incorporates spatial and gray level information to guarantee noise insensitiveness and image detail preservation. In [12], Gong et al. proposed a reformulated fuzzy local-information c-means for classifying changed and unchanged regions, which incorporates the information about spatial context by adding a new fuzzy factor into its objective function for the purpose of enhancing the changed information and reducing the effect of speckle noise. In [14], Gong et al. proposed a other new SAR images change detection approach based on FCM algorithm by adding Markov random field with a novel form of energy function (MRFFCM).

☆ This work was supported by the National Natural Science Foundation of China (Grant Nos. 61273317 and 61422209), the National Top Youth Talents Program of China, the Specialized Research Fund for the Doctoral Program of Higher Education (Grant No. 20130203110011) and the Fundamental Research Fund for the Central Universities (Grant No. K5051202053).

* Corresponding author. Tel.: +86 029 88202661; fax: +86 029 88201023.
E-mail address: gong@ieee.org (M. Gong).

http://dx.doi.org/10.1016/j.asoc.2015.10.044
1568-4946/

These algorithms have taken the spatial context information into consideration to suppress the effect of speckle noise to a certain degree [18,20,12]. However, these methods have the same shortcoming that they all require an artificial selection of a crucial parameter which indicates a trade-off between the capabilities of detail preserving and noise removing. In fact, change detection is inherently a multiobjective task for the contradiction between removing noise and preserving detail. However, in traditionary change detection methods, either only one of the objectives is adopted as the cost function or multiple objectives are aggregated to a scalar cost function. There are two main weaknesses if a scalarized objective function is used. First, the determination of an appropriate parameter reflects the purpose of the user is difficult without a priori knowledge about the existing noise in images. Second, only a single solution can be obtained, from which little insight into the problem can be gained.

In this paper, we propose a completely novel approach for change detection in SAR images by using a multiobjective fuzzy clustering method, which is denoted as MOFCM for short. It models the change detection problem as a multiobjective optimization problem (MOP). The essence of the MOP is to optimize several conflicting objectives simultaneously. An improvement of one objective may result in the performance degradation of other objectives. It is impossible to achieve optimal effects of all the multiple targets at the same time, so a trade-off is needed to achieve the approximate optimal solutions for each objective as far as possible. In MOFCM, on one hand, we construct two objective functions from the perspective of preserving detail and removing noise, and ultimately transform the change detection problem into a MOP. On the other hand, we optimize the two constructed objective functions simultaneously by using a multiobjective fuzzy clustering method. The contribution of this paper is threefold: (1) We model the change detection problem as a MOP for considering of preserving detail and restrain noise. (2) We propose a multiobjective clustering algorithm for change detection to optimize the two objectives simultaneously. The proposed method decomposes this MOP into a number of scalar problems with different weight values and then updates the membership values of each pixel according to the weight values of subproblems. In this way, the objective function is no longer a scalar value, but a vector. Then the cluster centers are updated by using evolutionary algorithms to increase the probability of converging to the global optimal solution. (3) A set of solutions are obtained by the proposed method to gain more insights into the change detection problems. The aforementioned issues existed in traditional change detection methods can thus be alleviated.

The rest part of this paper is organized as follows. Section 2 introduces the related background and the motivation of the proposed MOFCM for change detection in SAR images. Meanwhile, the details for the proposed MOFCM will be displayed in Section 3. Experimental study and conclusions will be presented in Sections 4 and 5, respectively.

2. Related background and motivation

In this section, in order to make it easier to understand the proposed method, we will give a brief introduction to evolutionary multiobjective optimization. Then we will state our motivation for modeling change detection problem as a MOP.

2.1. Introduction to evolutionary multiobjective optimization

In general, a MOP is composed of several decision variables, objective functions, and some constraint conditions [22,23]. A MOP can be defined as:

$$\begin{aligned} &\min F(x) = (f_1(x), \ldots, f_k(x))^T \\ &\text{subject to } x \in \Omega, \end{aligned} \tag{1}$$

where x is the decision vector, Ω is the decision space and k is the number of objective functions. It is worth noting that the MOP in Eq. (1) is a minimization problem.

In the case of minimization, let us assume that x_A and x_B are two decision vectors in the decision space Ω, x_A dominates x_B (denoted by $x_A \succ x_B$) if and only if

$$\begin{aligned} &\forall i = 1, 2, \ldots, k \quad f_i(x_A) \le f_i(x_B) \\ &\wedge \exists j = 1, 2, \ldots, k \quad f_i(x_A) < f_i(x_B). \end{aligned} \tag{2}$$

The decision vector $x^* \in \Omega$ is referred to as a nondominated solution when there is not another decision vector $x \in \Omega$ dominating it. The set of Pareto optimal solutions is called the Pareto optimal set, and it is expressed as:

$$P^* \triangleq \{x^* \in \Omega | \neg \exists x \in \Omega, x \succ x^*\}. \tag{3}$$

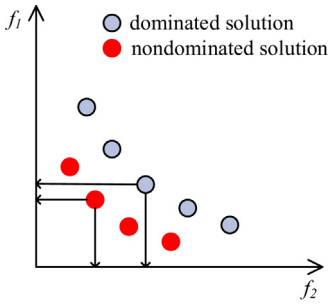

Fig. 1. The distributions of dominated solutions and nondominated solutions in the objective space of the two-objective problem.

In order to illustrate the concept of nondominated solutions, we take a two-objective minimization problem as an example. Fig. 1 shows the distributions of the dominated solutions and nondominated solutions in the objective space. All the objective function vectors corresponding to all Pareto optimal points constitute a Pareto-optimal front (PF) which is expressed as:

$$PF^* \triangleq \{F(x^*) = (f_1(x^*), f_2(x^*), \ldots, f_k(x^*))^T | x^* \in P^*\}. \tag{4}$$

Algorithm 1. Algorithm of MOEA/D.

Step 1) Initialization
Step 1.1) Generate an equally distributed of n weight vectors $w^1, w^2, \ldots, w^n$.
Step 1.2) Work out the T closest weight vectors to each weight vector.
Step 1.3) Randomly generate an initial population $x^1, x^2, \ldots, x^n$.
Step 2) Set $b = 0$.
Step 3) Cycling
for $i = 1, 2, \ldots, n$, **do**
  Step 3.1) Select mating parents from the neighborhood.
  Step 3.2) Generate new solution y by using a specific genetic operator.
  Step 3.3) Update the population.
end for
Step 4) Stopping criteria: t is the maximum number of generations. If $b < t$, then b++ and go to **Step 3**, otherwise, stop the algorithm and output.

For multi-objective optimization, it has been recognized that evolutionary algorithms (EAs) are well suited because EAs can deal with a set of possible solutions simultaneously [22]. Since [24], various EAs to deal with MOPs have been proposed such as [25–27] and these EAs are termed as multi-objective evolutionary algorithms (MOEAs). MOEAs seek to obtain a set of Pareto optimal solutions for approximating the true PF in a single run. MOEA/D proposed by Zhang and Li [27] has obtained a good performance in multiobjective optimization. It decomposes a MOP into a set of scalar optimization subproblems and optimizes them simultaneously. Each subproblem is optimized by only using information from its several neighboring subproblems. The procedure of MOEA/D is shown in Algorithm 1. The proposed change detection method uses MOEA/D as the underlying optimization tool.

2.2. Motivation of converting the change detection problem into a MOP

For change detection in SAR images, many changes are false or remain undetected because of the speckle noise [28]. The source of speckle noise can be attributed to random interference between the coherent returns issued from the numerous scatterers present on a surface. Speckle noise manifests itself in the form of a random pixel-to-pixel variation with statistical properties similar to those of thermal noise and makes it difficult to visually and automatically interpret SAR data [29]. Due to the fact that SAR images

suffer from the presence of the speckle noise, it is rather difficult to keep trade-off between robustness to noise and effectiveness of preserving the details. In [5,6], a multilevel representation of the multitemporal information was computed by decomposing the log-ratio image into several images of the same size as the original one to reduce the noise impact. Bzai et al. [8] used the generalized Gaussian distribution to model the changed and unchanged classes to reduce the corruption of the speckle noise. Furthermore, many probability density functions such as Log normal, Generalized Gaussian, Nakagami ratio, and Weibull ratio were investigated to model the distribution of the two classes in [9]. In [10], Hu et al. presented an automatic and effective approach to the thresholding of the log-ratio change indicator whose histogram may have one mode or more than one mode. Moreover, many researchers have added local or non-local information into their algorithms to make them robust to noise [12–14].

Due to the fact that SAR images suffer from the presence of the speckle noise, it is an urgent task to keep trade-off between robustness to noise and effectiveness of preserving the details. Therefore the change detection problem can be modeled as a MOP for the contradiction between removing noise and preserving detail. In this paper, a multi-objective clustering algorithm for change detection in SAR images is proposed to address the issues existed in the traditional change detection methods. It models the change detection problem as a MOP and considers the image detail preserving capability and noise removing capability as two different objectives. This paper obtains different solutions by decomposing this MOP into a number of scalar optimization subproblems with different weight values and optimizing these subproblems with evolutionary algorithms. It is worth mentioning that each solution in the PF indicates a trade-off between the capabilities of detail preserving and noise removing to a certain degree, which can meet the different requirements of users.

3. Methodology

As is mentioned in Section 1, image change detection is based on the comparative analysis of two images acquired from the same area at different times with the purpose of detecting the change regions between them. Generally speaking, an image change detection method is mainly composed of three steps: (1) image preprocessing; (2) the acquisition of the difference image between the two images remaining to be detected; and (3) analysis of the difference image. In our MOFCM, we focus our major attention on the last two steps and its schematic diagram is shown in Fig. 2. To summarize, the MOFCM is carried out as the following steps:

Step 1: Generate a difference image by applying a change detection operator to multitemporal images remaining to be detected.
Step 2: Generate a de-noised difference image by executing a filtering processing on the image generated in step 1.
Step 3: Construct two objective functions corresponding to detail preserving and noise removing capability.
Step 4: Model the change detection problem as a MOP by using the previous two objective functions.
Step 5: Solve the MOP and obtain a PF by using MOFCM.
Step 6: Display all the final change detection binary maps corresponding to each solution in the PF.

3.1. Generation of difference images

Here we let I_1 and I_2 are separately two original images acquired by a SAR over the same geographical area but at two different times t_1 and t_2. And they have the same size of $A \times B$. Then, we apply the frequently-used log-ratio operator to the two original images to create a difference image I_l which preserves the image detail well. It can be obtained as follows:

$$I_l = \left|\log\left(\frac{I_2}{I_1}\right)\right| = |\log I_2 - \log I_1|. \tag{5}$$

Further on, a filtering processing is required to apply to the difference image I_l in order to remove noise, and then we get a de-noised image which has been removed most the image noise. In our method, we employ the neighbour average filtering to implement this procedure and obtain the image I_n as the following formula:

$$\overline{x_i} = \frac{1}{S}\sum_{i \in N_r} x_i, \tag{6}$$

where $\overline{x_i}$ and x_i are the gray values of the ith pixel of image I_n and I_l, respectively, N_r represents a set of neighbors falling into a window of fixed size around x_i, S stands for the total number of set N_r.

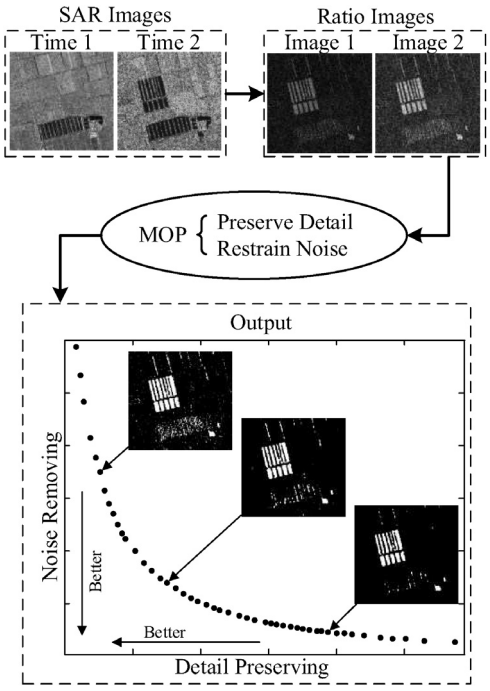

Fig. 2. Schematic diagram of the proposed MOFCM.

3.2. Two objective functions constructed for multiobjective optimization

As described in Section 1, in MOFCM, the change detection problem is transformed into a MOP. Firstly, from the perspective of preserving image detail, FCM is applied directly to the difference image I_l generated from two original images. We consider the cost function of FCM as our first objective function for the MOP since the image I_l contains lots of details, which is defined as:

$$f_1(v_1, v_2) = \sum_{i=1}^{N}\sum_{k=1}^{c} u_{ki}^m \|x_i - v_k\|^2, \tag{7}$$

where N is the total number of pixels, c stands for the number of clusters, m is a fuzzy exponent and usually selected as 2, u_{ki} is the fuzzy membership degree of the ith pixel with respect to cluster k with $0 \le u_{ki} \le 1$ and $\sum_{k=1}^{c} u_{ki} = 1, \forall i = 1, 2, \ldots, N$, and v_k is the average gray value of the center of cluster k. For our change detection problem, we divide the image into unchanged and changed

classes, so c is equal to 2. Moreover, the cluster center v_k is obtained by initializing randomly and the fuzzy membership degree u_{ki} is calculated by using a derived formula with respect to the cluster center v_k.

On the other hand, from the perspective of removing noise, the same cluster analysis is exerted on the de-noised image, and the corresponding cost function is defined as:

$$f_2(v_1, v_2) = \sum_{i=1}^{N}\sum_{k=1}^{c} u_{ki}^m \|\overline{x_i} - v_k\|^2. \tag{8}$$

At this point, the two objective functions can be combined into a MOP. It has the following form:

$$\begin{aligned} &\min F(v_1, v_2) = (f_1, f_2)^T \\ &\text{s.t.} \quad (v_1, v_2)^T \in \Omega, \end{aligned} \tag{9}$$

where $(v_1, v_2)^T$ is a decision vector consisting of the two cluster centers v_1 and v_2, Ω is the decision space of the MOP. As we all know, the fundamental principle of FCM clustering is to acquire a good classification result by minimizing its cost function. Hence, the MOP will be solved as a minimization problem. From all the above, it is reasonable to conclude that a smaller f_1 indicates a better detail preserving capability while a smaller f_2 means a better noise removing capability.

3.3. Multiobjective fuzzy clustering for change detection

In this paper, MOEA/D is employed in the proposed MOFCM as the underlying optimization tool. In MOFCM, we obtain each scalar optimization subproblem as the following form in Eq. (10) by applying the weighted sum decomposition approach to the newly combined MOP:

$$\begin{aligned} &\min g^{ws}(v|\overline{w}) = w_1 f_1 + w_2 f_2 \\ &\text{s.t.} \quad (v_1, v_2)^T \in \Omega, \end{aligned} \tag{10}$$

where $\overline{w} = (w_1, w_2)^T$ is a weight vector with $w_1, w_2 \geq 0$ and $w_1 + w_2 = 1$, $g^{ws}(v|\overline{w})$ stands for a newly decomposed problem. Likewise, we can get a set of subproblems like this by selecting different weight vector $\overline{w}$ in Eq. (10). Each different weight vector $\overline{w}$ represents a certain trade-off between the capabilities of image detail preserving and noise removing. When $w_1 > w_2$, the effect of image detail preserving is better than that of noise removing and vice versa.

The proposed MOFCM algorithm for image change detection is given in Algorithm 2. The change detection problem in (9) can be decomposed into n subproblems by Eq. (10). In the initialization, we define a well-distributed weight vectors $w^1, w^2, \ldots, w^n$ and work out the T closet weight vectors to each weight vector. Then a population $P = \{v^1, v^2, \ldots, v^n\}$ is randomly generated, where v represents the cluster centers of changed and unchanged regions. During iterations, MOEA/D uses a specific genetic operator for producing an offspring from its several neighboring solutions. Then the offspring is used to update the neighboring solutions. At the end of MOFCM, a set of solutions with different trade-off relationships between preserving details and restraining noise are obtained to gain more insights into the change detection problem.

Algorithm 2. Algorithm of the proposed MOFCM for change detection.

Input: n: the number of subproblems, T: neighborhood size, t: the maximum number of generations, pc: the probability of crossover, pm: the probability of mutation.
Output: Pareto front solutions. Each solution corresponds to a change detection result map.

1: **Step 1) Initialization**
2: **Step 1.1)** Generate an equally distributed of n weight vectors $w^1, w^2, \ldots, w^n$ and compute the Euclidean distances between any two weight vectors and then work out the T closest weight vectors to each weight vector. For $i = 1, 2, \ldots, n$, set $B(i) = \{i_1, \ldots, i_T\}$, where $\lambda^{i_1}, \ldots, \lambda^{i_T}$ are the T closest weight vectors to λ^i.
3: **Step 1.2)** Randomly generate an initial population $v^1, v^2, \ldots, v^n$.
4: **Step 1.3)** Calculate the fuzzy membership matrix $u^1, u^2, \ldots, u^n$ by Eq.(12) and calculate $f_1, f_2, g^{ws}(v^i|\overline{w})$.
5: **Step 2)** Set $b = 0$.//the number of flight cycles
6: **Step 3) Cycling**
7: **for** $i = 1, 2, \ldots, n$, **do**
8: **Step 3.1)** Select two subscripts s, l from $B(i)$, and then produce a new individual solution y from v^s and v^l by using a specific genetic operator with pc and pm. For more information, please refer to [27].
9: **Step 3.2)** Obtain the new fuzzy membership matrix u^y by Eq. (12) with new solution y.
10: **Step 3.3)** Calculate $g^{ws}(y|\overline{w})$. For each $j \in B(i)$, if $g^{ws}(y|\overline{w}) \leq g^{ws}(v^j|\overline{w})$, then we set $v^j = y$ and $g^{ws}(v^j|\overline{w} = g^{ws}(y|\overline{w})$.
11: **end for**
12: **Step 4) Stopping criteria**: If $b < t$, then b++ and go to **Step 3**, otherwise, stop the algorithm and output.

In this paper, the idea of decomposition is also used in the process of updating the membership values. Decomposition transforms the MOP into a set of distinct scalar aggregation problems. Next, a new objective function is constructed by applying Lagrange multiplier method to each subproblem and the newly constructed objective function is shown as follows:

$$\begin{aligned} &\overline{g^{ws}}(U, v, \lambda_1, \ldots, \lambda_N|\overline{w}) \\ &= (w_1 f_1 + w_2 f_2) + \sum_{i=1}^{N}\lambda_i \left(\sum_{k=1}^{2} u_{ki} - 1\right) \\ &= \sum_{i=2}^{N}\sum_{k=1}^{2} u_{ki}^m \|x_i - v_k\|^2 + \sum_{i=2}^{N}\sum_{k=1}^{2} u_{ki}^m \|\overline{x_i} - v_k\|^2 \\ &\quad + \sum_{i=1}^{N}\lambda_i \left(\sum_{k=1}^{2} u_{ki} - 1\right), \end{aligned} \tag{11}$$

where U is the membership degree matrix consisting of all the u_{ki}, and λ_i, $i = 1, 2, \ldots, N$ are Lagrange multipliers corresponding to all the constraint equations $\sum_{i=1}^{2} u_{ki} = 1$, $i = 1, 2, \ldots, N$. With that, we take the derivative with respect to each input parameter and obtain the necessary conditions for achieving the minimum value of each subproblem. One of the necessary conditions about the membership degree u_{ki} is described as follows:

$$u_{ki} = \frac{\left(\|x_i - v_k\|^2 + \frac{w_2}{w_1}\|\overline{x_i} - v_k\|^2\right)^{-1/(m-1)}}{\sum_{j=1}^{2}\left(\|x_i - v_j\|^2 + \frac{w_2}{w_1}\|\overline{x_i} - v_j\|^2\right)^{-1/(m-1)}}. \tag{12}$$

In this paper, two conflicting objective functions are optimized by the proposed algorithm simultaneously. The original membership updating formula of the standard FCM algorithm is not appropriate to update the membership values of each pixel. By using decomposition mechanism, this paper updates the membership values according to the weight values of each subproblem. The new membership updating formula makes full use of the information of the log-ratio image and the filtered log-ratio image.

The complexity of each scalar optimization could scale up with the number of decision variables [27]. In this paper, the decision variables are the cluster centers of changed and unchanged regions. The number of decision variables is 2. Therefore the complexity of the proposed method is not high. Furthermore, in order to be robust to noise, a neighborhood function is often used in change detection tasks. This function is calculated during iterations, which is time-consuming. In this paper, the neighborhood function is constructed

with a de-noised image, which can be computed in advance to reduce the computational cost.

4. Experimental study

In order to illustrate the effectiveness of our MOFCM, in this section, we will perform the MOFCM on four datasets of real world images with different characteristics in the experiments. In the meantime, the experimental results of FCM, FCM_S1, and MRFFCM will also be presented to confirm the efficiency of MOFCM further.

4.1. Experimental datasets and evaluation indexes

The first dataset consists of two images with the size of 301×301 acquired over a region around Bern, the capital city of Switzerland, in April and May 1999, respectively. Between the two dates, the River Aare inundated parts of Bern and Thun and the whole airport in Bern. As a result, the valley between Bern and Thun is chosen as a test place for determining the regions flooded. The two images and the available ground truth image acquired by integrating photo interpretation with prior information are shown in Fig. 3.

The second dataset is the Ottawa dataset, they are offered by the Defence Research and Development Canada Ottawa. It contains two SAR images with the size of 290×350 acquired by a sensor called RADARSAT SAR. These images have been registered by a specific algorithm in advance. The two images and corresponding available ground truth are shown in Fig. 4.

The third and fourth data sets are parts of the Yellow River Estuary dataset including two SAR images acquired by Radarsat-2 at the region of Yellow River Estuary in China in June 2008 and June 2009, respectively. The original size of these two images is 7666×7692. They are too large to be shown as the whole ones in such a small page. Therefore, we select two representative parts of size 306×291 and 291×444 respectively in the experiments. The two parts selected from the Yellow River dataset and their corresponding ground truth images are presented in Figs. 5 and 6, respectively. In addition, it is worth noting that one of the two original images is a single-look image and the other is a four-look image. This implies that speckle noise affects the image taken in 2009 more seriously than that taken in 2008. Such a difference in speckle noise level between the two images is likely to exacerbate the difficulties in change detection.

Generally speaking, there are two manners to account for the effects of SAR image change detection problems. A visual way is used to show the final change detection binary maps. The other way is to calculate the values of some common indexes for evaluation. In our experiments, percentage of correct classification (PCC) and Kappa coefficient are considered as the primary evaluation indexes. The Kappa coefficient is a measurement of consistency and accuracy on the basis of error matrix, and its value falls usually into the interval [0,1]. It is equal to 1 when the final binary map is coincided completely with the image of ground truth. In the following,

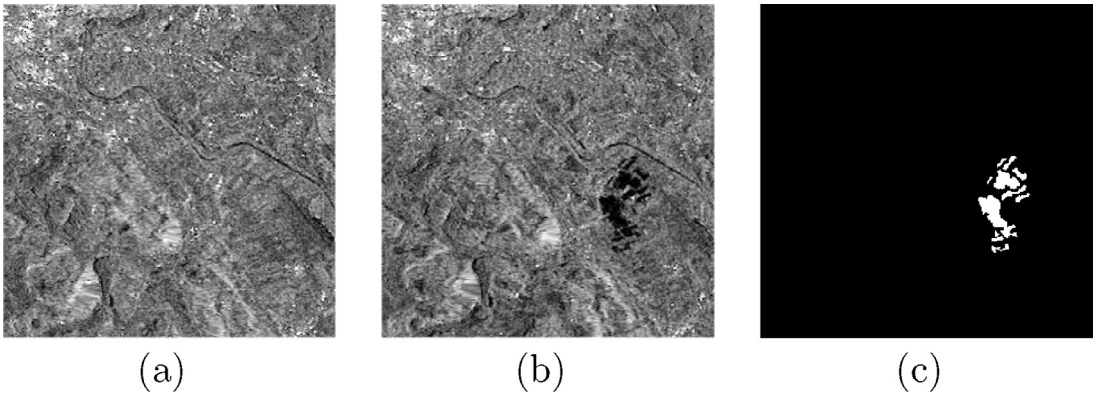

Fig. 3. Images for Bern dataset. (a) Image acquired in April 1999. (b) Image acquired in May 1999. (c) Image of the ground truth.

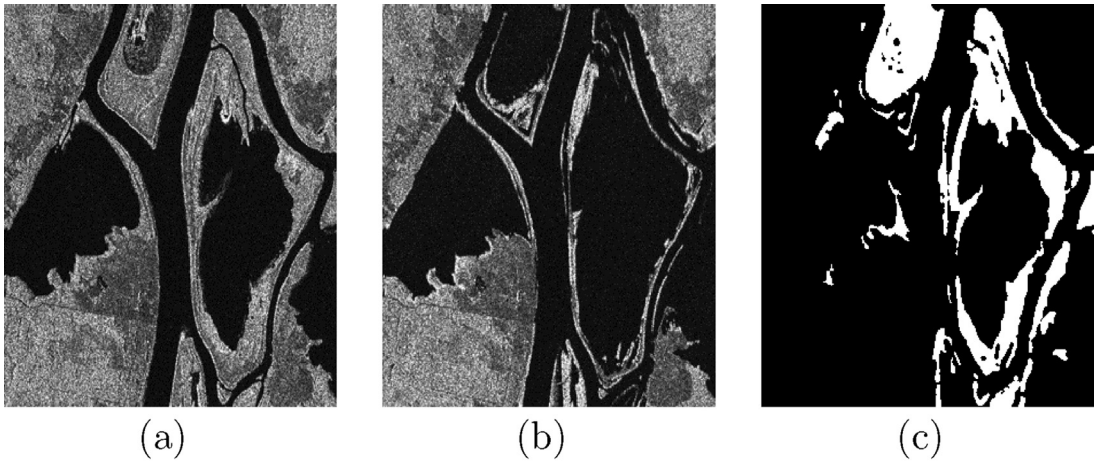

Fig. 4. Images for Ottawa dataset: (a) Image acquired in July 1997. (b) Image acquired in August 1997. (c) Image of the ground truth.

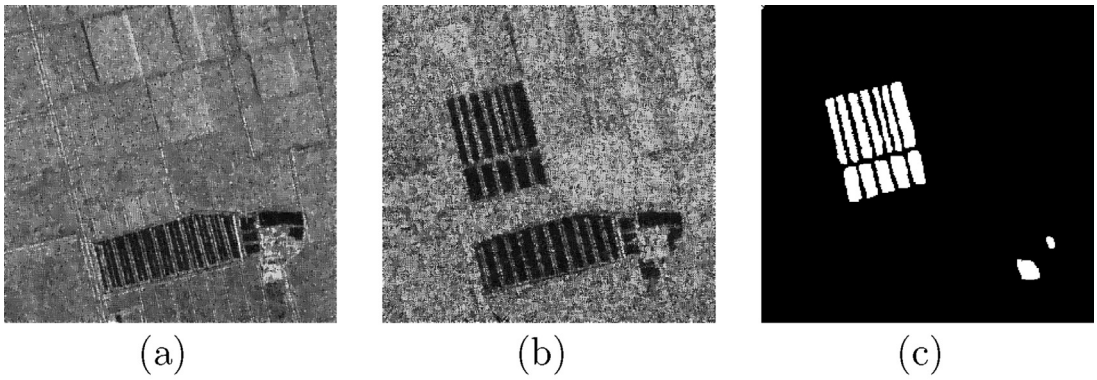

Fig. 5. Images for Yellow River I dataset: (a) Image acquired in June 2008. (b) Image acquired in June 2009. (c) Image of the ground truth.

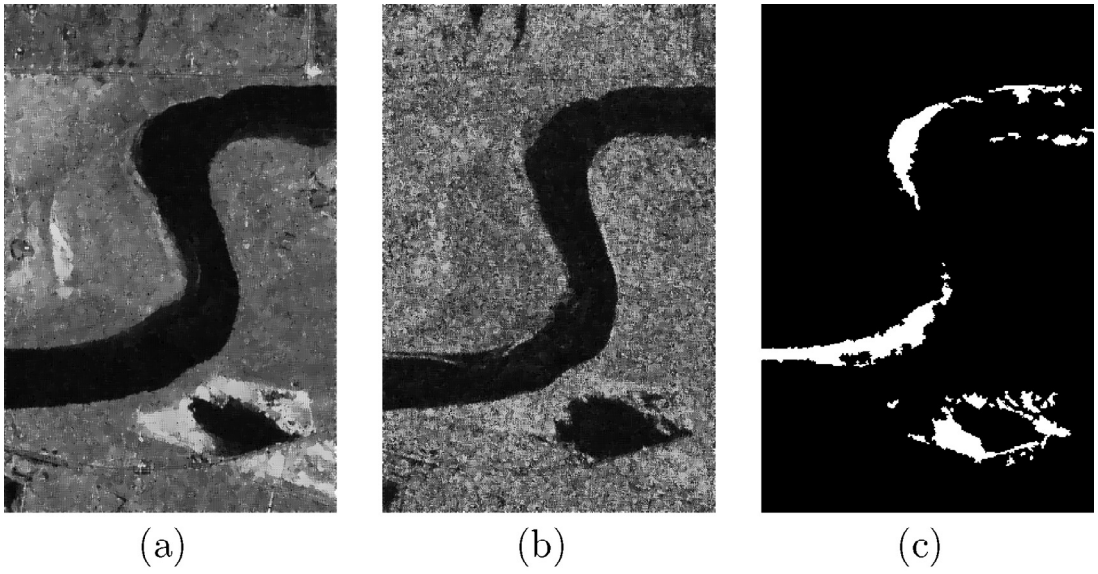

Fig. 6. Images for Yellow River II dataset: (a) Image acquired in June 2008. (b) Image acquired in June 2009. (c) Image of the ground truth.

we will display the calculation formulations of the PCC and Kappa coefficient in Eqs. (13) and (14):

$$PCC = \frac{TP + TN}{N}, \tag{13}$$

$$Kappa = \frac{PCC - PV}{1 - PV}, \tag{14}$$

where

$$PV = \frac{(TP + FP) \cdot RC + (TN + FN) \cdot RU}{N^2}, \tag{15}$$

where FP and FN stand for the number of pixels being unchanged in the ground truth but falsely detected as changed in the final binary map and of pixels being changed but falsely detected as unchanged, TP and TN are the number of changed pixels and of unchanged pixels in both the ground truth and final binary map, RC and RU represent the number of real changed pixels and of real unchanged pixels in the ground truth, and N is the total number of pixels in final binary map as well as the ground truth.

4.2. Experimental results

For the four datasets, we select a 3×3 window to implement the neighbour average filtering, thus getting the de-noised difference images. Meanwhile, the experiment parameters in MOFCM are displayed in Table 1. After applying our MOFCM to the Bern dataset, we get a uniformly-distributed PF including one hundred Pareto optimal solutions with different effects of detail preserving and noise removing. The PF for Bern dataset is shown in Fig. 7(a). We select six points (a-f) from it and display their corresponding final change detection maps in Fig. 8. The weight vectors corresponding to the six maps in Fig. 8(a)–(f) are $(0, 1)^T$, $(0.15, 0.85)^T$, $(0.3, 0.7)^T$, $(0.5, 0.5)^T$, $(0.8, 0.2)^T$, and $(1, 0)^T$. By comparing the six images in Fig. 8, we can find the fact that Fig. 8(a) and (b) contain less noise than the other four maps but fail to detect some crucial changed regions. However, Fig. 8(e) and (f) have detected more changed regions but include much noise. Fig. 8(c) and (d) indicate

Table 1
The parameters in the MOFCM used in the experiments.

Parameter	Meaning	Value
n	The number of subproblems	100
T	The number of neighbors	20
t	The maximum of generations	100
pc	The probability of crossover	0.5
pm	The probability of mutation	0.01

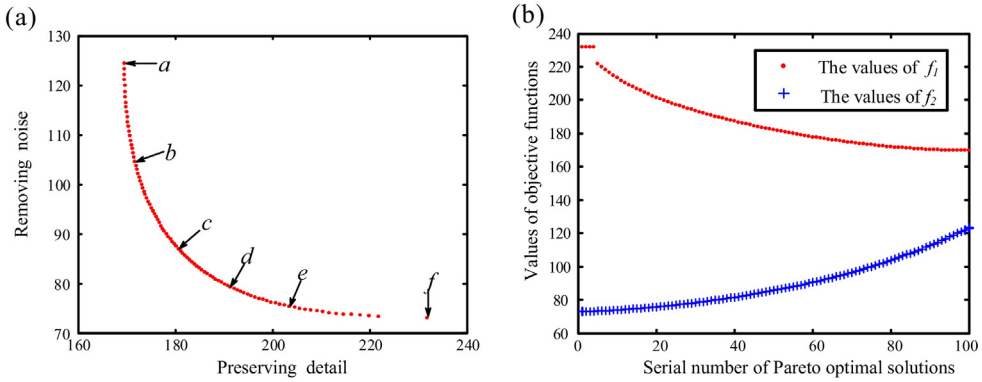

Fig. 7. Bern dataset. (a) The PF. (b) The values of two objective functions corresponding to the solutions in (a).

that the effects of detail preserving and noise removing fall in between the two cases above. All these phenomena show that all the solutions have different detail preserving and noise removing capabilities. Fig. 7(b) shows the changing trends of the capabilities of detail preserving and noise removing of the 100 solutions. The vertical coordinates of red points represent the first objective function values corresponding to each solution. The blue points represent the second objective function values corresponding to each solution. The smaller the corresponding objective function value is, the better the detail preserving or noise removing capability is.

Similarly, we employ our MOFCM to deal with the Ottawa dataset and reach its evenly-distributed PF present in Fig. 9(a). The set of PF is also composed of one hundred Pareto optimal solutions with different effects of detail preserving and noise removing. Six different change detection maps selected from the set are shown in Fig. 10. It is obvious that there are less speckle noise than the other four maps in Fig. 10(a) and (b). But some real changed regions are not detected in these maps. On the other hand, more changed regions are detected successfully while more noises are left in Fig. 10(e) and (f), which manifests a weaker noise removing capability but a better detail preserving capability in this case. In addition, the objective function values corresponding to the 100 solutions to the Ottawa dataset is shown in Fig. 9(b), which indicates the changing trends of the capabilities of detail preserving and noise removing of them.

Finally, we conduct an experiment on the two datasets selected from the original Yellow River dataset by using MOFCM. And their corresponding PF are shown in Figs. 11(a) and 13(a), respectively. The two datasets are different from Bern and Ottawa dataset, they own characteristics result in more difficulties in change detection. It is obvious that their PFs in Figs. 11(a) and 13(a) are

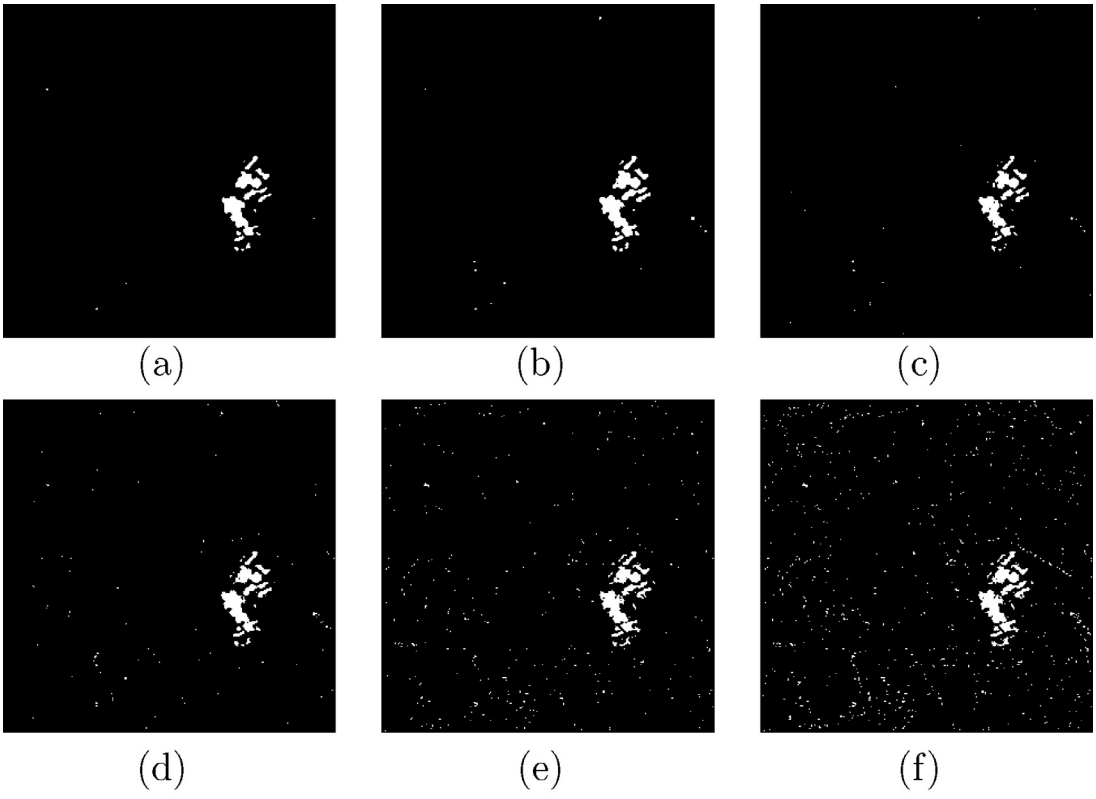

Fig. 8. Six different change detection maps selected from all the 100 results of the Bern dataset.

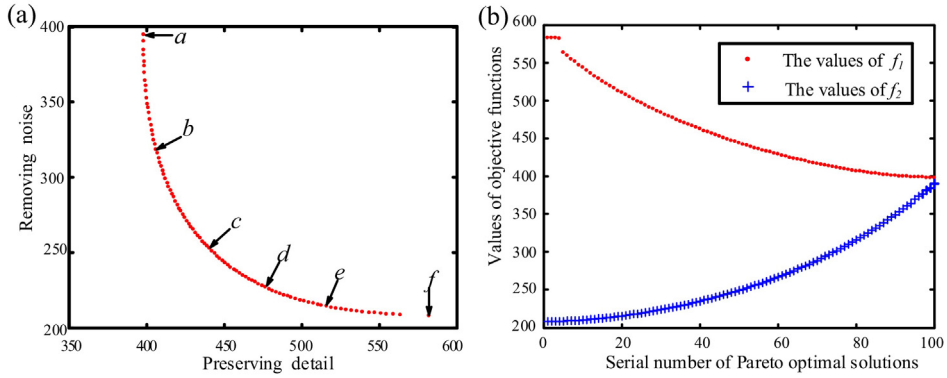

Fig. 9. Ottawa dataset. (a) The PF. (b) The values of two objective functions corresponding to the solutions in (a).

also even-distributed. In the same way, the set of PF for each Yellow River dataset is also composed of one hundred solutions with different effects of detail preserving and noise removing. Six corresponding different change detection maps selected from each set are shown in Figs. 12 and 14, respectively. The objective function values corresponding to the 100 solutions to each dataset are respectively displayed in Figs. 11(b) and 13(b), which also indicate the changing trends of the capabilities of detail preserving and noise removing of them.

Furthermore, for each dataset, we run the program of our MOFCM 30 times and plot the corresponding box plots which show the statistic results of the best PCC and Kappa in each generation. A Box plot displays the differences between populations under no assumptions of the underlying statistical distribution. The spacings between the different parts of the plot box can help reflect the degree of dispersion and skewness in the data, and identify outliers. In other words, the box plots can indicate the stability of MOFCM. The box plots of the statistical values of the best PCC and Kappa over 30 times running on the four datasets are shown in Fig. 15. In each box plot, the red line represents the median, the edges of each box are upper and lower quartiles, the whisker extends to the minimum and maximum points which are not considered as outliers,

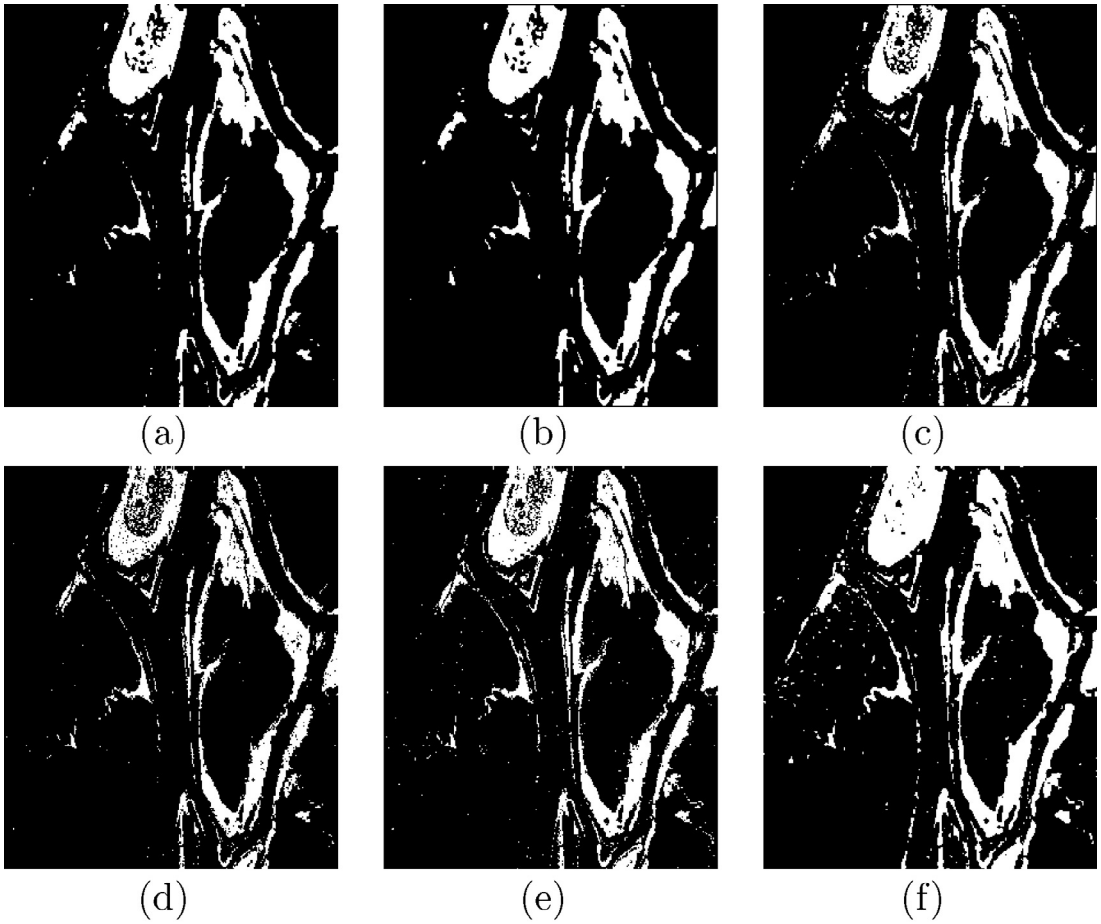

Fig. 10. Six different change detection maps selected from all the 100 results of the Ottawa dataset.

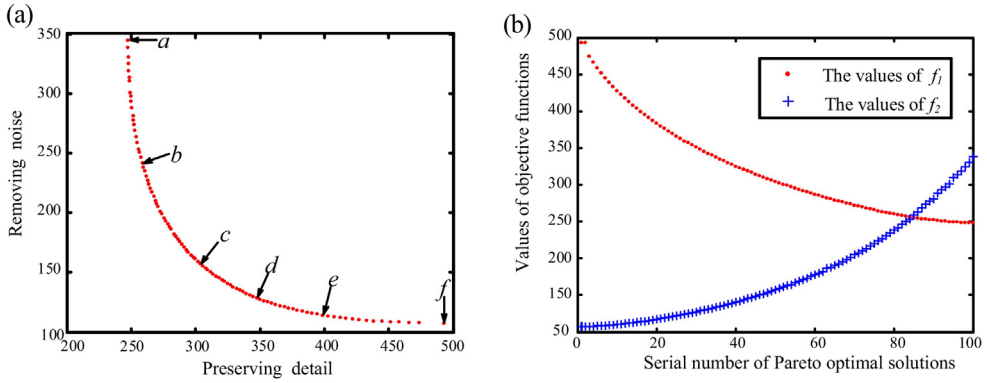

Fig. 11. Yellow River I dataset. (a) The PF. (b) The values of two objective functions corresponding to the solutions in (a).

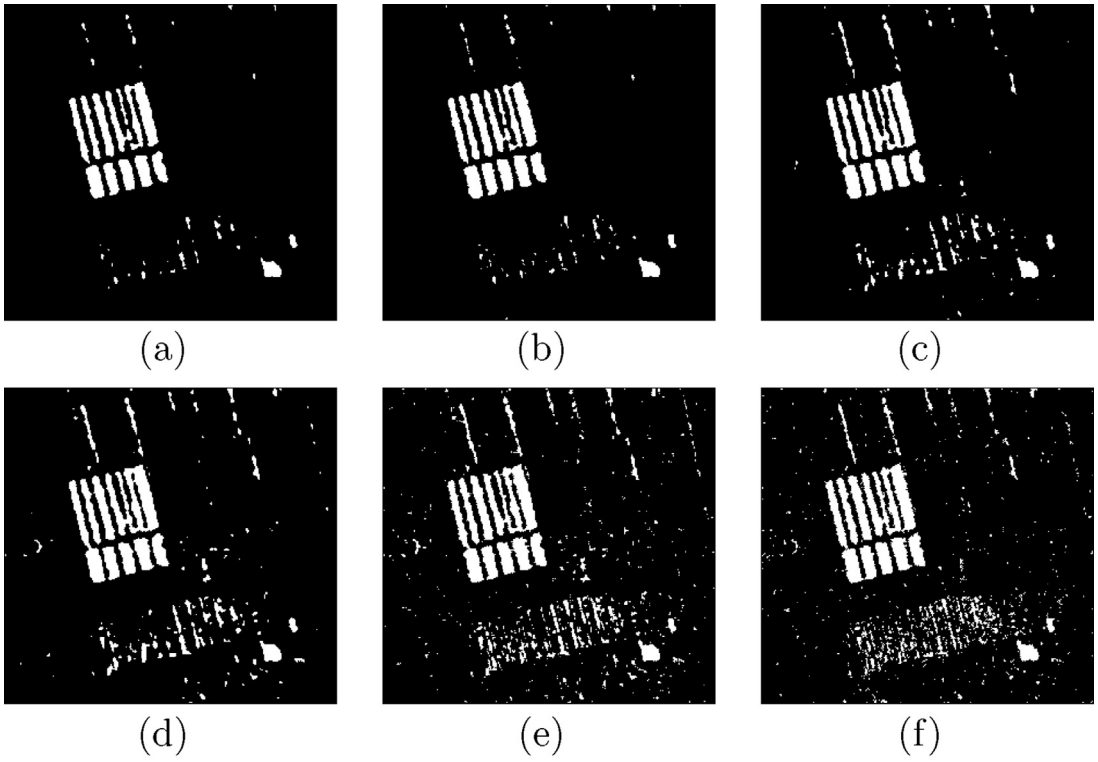

Fig. 12. Six different change detection maps selected from all the 100 results of the Yellow River I dataset.

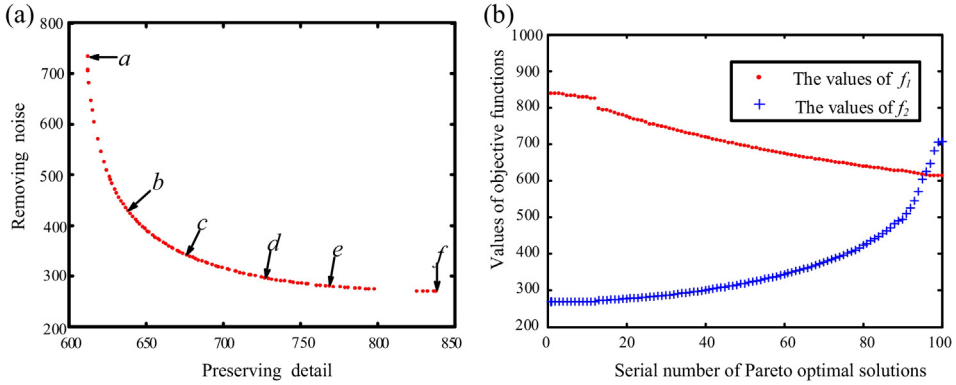

Fig. 13. Yellow River II dataset. (a) The PF. (b) The values of two objective functions corresponding to the solutions in (a).

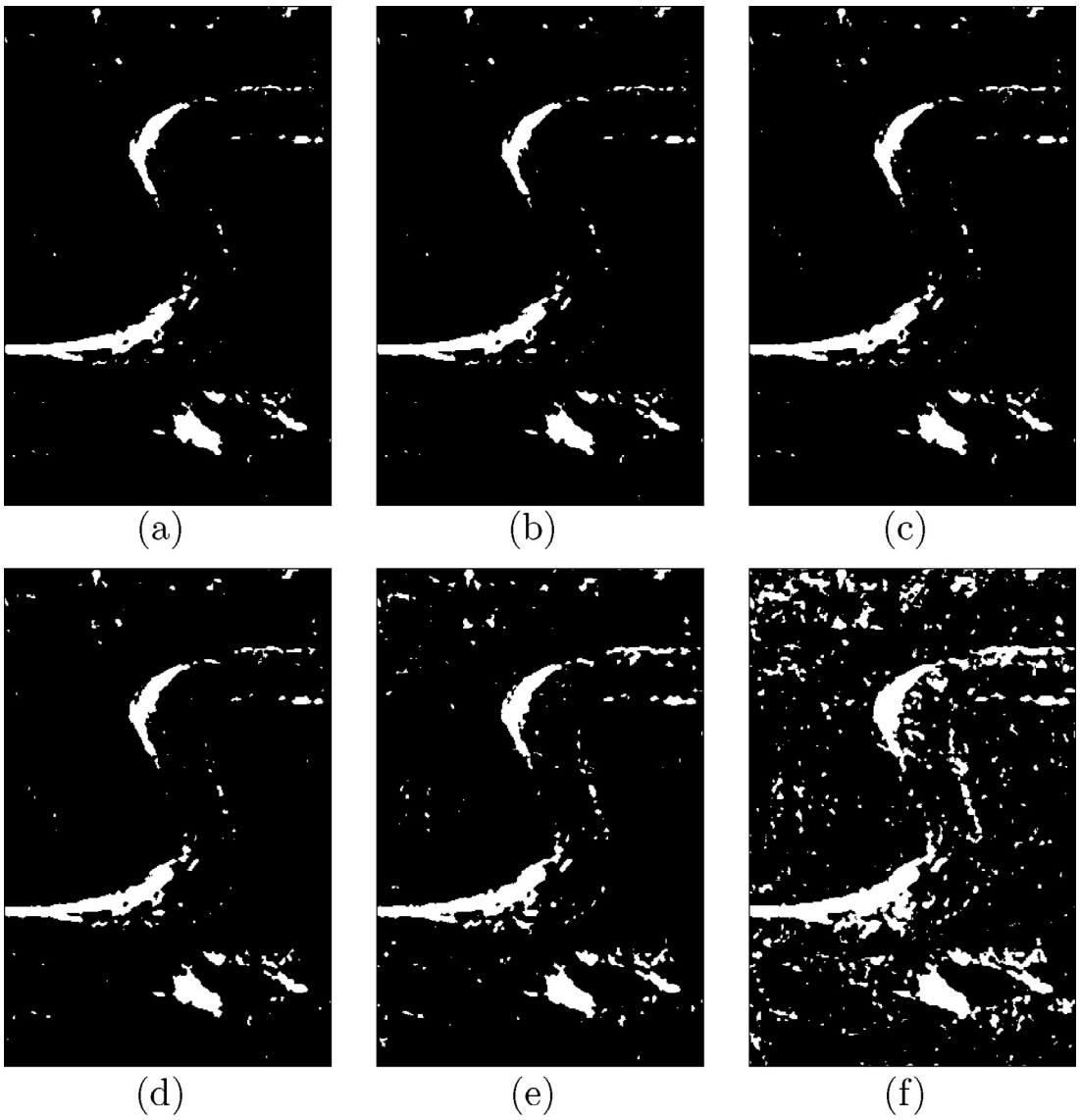

Fig. 14. Six different change detection maps selected from all the 100 results of the Yellow River II dataset.

and the outliers are plotted individually. Symbol + denotes outliers. From Fig. 15, for each dataset, the variation of the values of PCC and Kappa calculated over the 30 times running is fairly small, which indicates a good stability of MOFCM.

In order to demonstrate the availability of MOFCM in depth, we calculate the average values of the best PCC and Kappa over 30 times running, and the results are recorded in Table 2. For comparison, the results of FCM, FCM_S1, and MRFFCM on the same datasets are also listed in Table 2. By comparing the values of PCC and Kappa obtained by MOFCM with those of FCM, FCM_S1, and MRFFCM, we can conclude that our MOFCM can obtain better results.

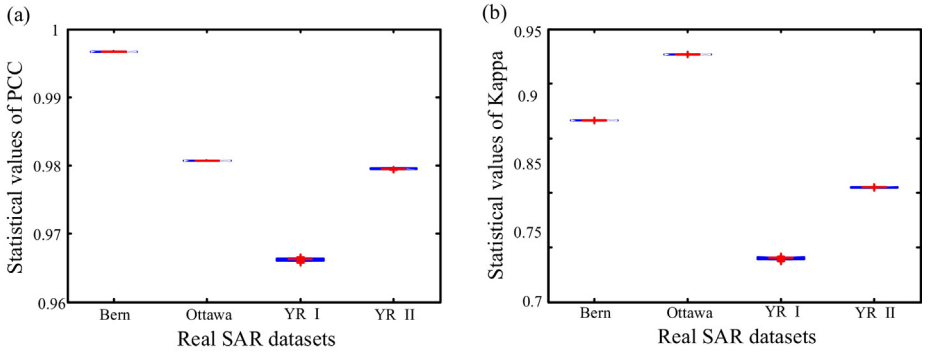

Fig. 15. Box plot of the statistical values of the best PCC and Kappa over 30 times running on the four datasets.

Table 2
The results obtained by four methods on the four datasets.

Datasets	Index	FCM	FCM_S1	MRFFCM	MOFCM
Bern	Kappa	0.7000	0.8304	0.8413	0.8666
	PCC	0.9920	0.9957	0.9955	0.9967
Ottawa	Kappa	0.8185	0.8797	0.9151	0.9268
	PCC	0.9524	0.9694	0.9769	0.9807
Yellow River I	Kappa	0.3143	0.5964	0.7283	0.7398
	PCC	0.8318	0.9367	0.9532	0.9662
Yellow River II	Kappa	0.2638	0.4832	0.7822	0.8050
	PCC	0.8026	0.9047	0.9504	0.9795
Mean	Kappa	0.5242	0.6974	0.8167	0.8346
	PCC	0.8947	0.9516	0.9690	0.9808

5. Concluding remarks

In this paper, a multiobjective fuzzy clustering method has been proposed for change detection in SAR images. It converted the change detection problem into a MOP by considering the image detail preserving and noise removing as two separate objectives. Inspired by the idea of decomposition, the proposed method decomposed this MOP into a number of scalar problems with different weight values and then updated the membership values of each pixel according to the weight values of subproblems. As a consequence, the proposed MOFCM could obtain a set of solutions with different detail preserving capability and noise removing capability to gain more insights into the change detection problem. Experimental results demonstrated the effectiveness and stability of the MOFCM for images with distinct features. Compared with those existing methods belonging to single objective optimization, MOFCM as a multiobjective optimization method was more suitable for dealing with the conflict between removing noise and preserving detail in the process of SAR images change detection.

References

[1] R.J. Radke, S. Andra, O. Al-Kofahi, B. Roysam, Image change detection algorithms: a systematic survey, IEEE Trans. Image Process. 14 (3) (2005) 294–307.
[2] L. Bruzzone, D.F. Prieto, An adaptive semiparametric and context-based approach to unsupervised change detection in multitemporal remote-sensing images, IEEE Trans. Image Process. 11 (4) (2002) 452–466.
[3] B. Hou, Q. Wei, Y. Zheng, S. Wang, Unsupervised change detection in SAR image based on Gauss-log ratio image fusion and compressed projection, IEEE J. Sel. Top. Appl. Earth Obs. Remote Sens. 7 (8) (2014) 3297–3317.
[4] J. Liu, M. Gong, Q. Miao, L. Su, H. Li, Change detection in synthetic aperture radar images based on unsupervised artificial immune systems, Appl. Soft Comput. 34 (2015) 151–163.
[5] F. Bovolo, C. Marin, L. Bruzzone, A hierarchical approach to change detection in very high resolution SAR images for surveillance applications, IEEE Trans. Geosci. Remote Sens. 51 (4) (2013) 2042–2054.
[6] C. Marin, F. Bovolo, L. Bruzzone, Building change detection in multitemporal very high resolution SAR images, IEEE Trans. Geosci. Remote Sens. 53 (5) (2014) 2664–2682.
[7] N.S. Mishra, S. Ghosh, A. Ghosh, Fuzzy clustering algorithms incorporating local information for change detection in remotely sensed images, Appl. Soft Comput. 12 (8) (2012) 2683–2692.
[8] Y. Bazi, L. Bruzzone, F. Melgani, An unsupervised approach based on the generalized Gaussian model to automatic change detection in multitemporal SAR images, IEEE Trans. Geosci. Remote Sens. 43 (4) (2005) 874–887.
[9] Y. Ban, O. Yousif, Multitemporal spaceborne SAR data for urban change detection in China, IEEE J. Sel. Top. Appl. Earth Obs. Remote Sens. 5 (4) (2012) 1087–1094.
[10] H. Hu, Y. Ban, Unsupervised change detection in multitemporal SAR images over large urban areas, IEEE J. Sel. Top. Appl. Earth Obs. Remote Sens. 7 (8) (2014) 3248–3261.
[11] V.-E. Neagoe, R.-M. Stoica, A.-I. Ciurea, L. Bruzzone, F. Bovolo, Concurrent self-organizing maps for supervised/unsupervised change detection in remote sensing images, IEEE J. Sel. Top. Appl. Earth Obs. Remote Sens. 7 (8) (2014) 3525–3533.
[12] M. Gong, Z. Zhou, J. Ma, Change detection in synthetic aperture radar images based on image fusion and fuzzy clustering, IEEE Trans. Image Process. 21 (4) (2012) 2141–2151.
[13] O. Yousif, Y. Ban, Improving SAR-based urban change detection by combining MAP-MRF classifier and nonlocal means similarity weights, IEEE J. Sel. Top. Appl. Earth Obs. Remote Sens. 7 (10) (2014) 4288–4300.
[14] M. Gong, L. Su, M. Jia, W. Chen, Fuzzy clustering with modified MRF energy function for change detection in synthetic aperture radar images, IEEE Trans. Fuzzy Syst. 22 (1) (2014) 98–109.
[15] O. Yousif, Y. Ban, Improving urban change detection from multitemporal SAR images using PCA-NLM, IEEE Trans. Geosci. Remote Sens. 51 (4) (2013) 2032–2041.
[16] M. Sezgin, et al., Survey over image thresholding techniques and quantitative performance evaluation, J. Electron. Imaging 13 (1) (2004) 146–168.
[17] M.N. Ahmed, S.M. Yamany, N. Mohamed, A.A. Farag, T. Moriarty, A modified fuzzy c-means algorithm for bias field estimation and segmentation of MRI data, IEEE Trans. Med. Imaging 21 (3) (2002) 193–199.
[18] S. Chen, D. Zhang, Robust image segmentation using FCM with spatial constraints based on new kernel-induced distance measure, IEEE Trans. Man Cybern. B: Cybern. 34 (4) (2004) 1907–1916.
[19] W. Cai, S. Chen, D. Zhang, Fast and robust fuzzy c-means clustering algorithms incorporating local information for image segmentation, Pattern Recognit. 40 (3) (2007) 825–838.
[20] S. Krinidis, V. Chatzis, A robust fuzzy local information c-means clustering algorithm, IEEE Trans. Image Process. 19 (5) (2010) 1328–1337.
[21] L. Szilagyi, Z. Benyo, S.M. Szilágyi, H. Adam, MR brain image segmentation using an enhanced fuzzy c-means algorithm, in: Proc. 25th Annu. Int. Conf. IEEE EMBS, vol. 1, 2003, pp. 17–21.
[22] K. Deb, Multi-objective Optimization Using Evolutionary Algorithms, Wiley, New York, 2001.
[23] C.A.C. Coello, D.A. Van Veldhuizen, G.B. Lamont, Evolutionary Algorithms for Solving Multi-objective Problems, Kluwer, Norwell, MA, 2002.
[24] J.D. Schaffer, Multiple objective optimization with vector evaluated genetic algorithms, in: Proc. 1st Int. Conf. Genetic Algorithms, 1985, pp. 93–100.
[25] K. Deb, A. Pratap, S. Agarwal, T. Meyarivan, A fast and elitist multiobjective genetic algorithm: NSGA-II, IEEE Trans. Evol. Comput. 6 (2) (2002) 182–197.
[26] C.A.C. Coello, G.T. Pulido, M.S. Lechuga, Handling multiple objectives with particle swarm optimization, IEEE Trans. Evol. Comput. 8 (3) (2004) 256–279.
[27] Q. Zhang, H. Li, MOEA/D: a multiobjective evolutionary algorithm based on decomposition, IEEE Trans. Evol. Comput. 11 (6) (2007) 712–731.
[28] R. Dekker, Speckle filtering in satellite SAR change detection imagery, Int. J. Remote Sens. 19 (6) (1998) 1133–1146.
[29] H. Xie, L. Pierce, F. Ulaby, SAR speckle reduction using wavelet denoising and Markov random field modeling, IEEE Trans. Geosci. Remote Sens. 40 (10) (2002) 2196–2212.